Water Air Soil Pollut (2012) 223:2551–2562
DOI 10.1007/s11270-011-1047-7

Adsorption of Phosphate by Amino-Functionalized and Co-condensed SBA-15

Jae-Woo Choi · Seung-Yeon Lee · Sang-Hyup Lee · Ki-Bong Lee · Dong-Ju Kim · Seok-Won Hong

Received: 28 July 2011 / Accepted: 8 December 2011 / Published online: 27 December 2011

Abstract In this study, the applications of mesoporous materials based on silica, and those with modifications, namely post-synthetic grafting, co-condensation, and pure SBA-15, were investigated for the removal of phosphate from sewage. The mesostructures were confirmed by X-ray diffraction, Brunauer–Emmett–Teller, Fourier transform infrared spectroscopy, and transmission electron microscopy. The absorption of phosphate by the mesoporous adsorbents was examined, using different adsorption models to describe the equilibrium and kinetic data. The maximum adsorption capacities of the mesostructured adsorbents were found to be 69.970, 59.890, and 2.018 mg/g for the co-condensation, post-synthetic grafting, and pure SBA-15, respectively. The kinetic data showed that the adsorption of phosphate onto three different mesostructures followed the pseudo-first-order kinetic model.

Keywords Amino-functionalized · Co-condensation · Grafting · Mesoporous silica · Phosphate · SBA-15

J.-W. Choi · S.-Y. Lee · S.-H. Lee · S.-W. Hong (✉)
Water Research Center,
Korea Institute of Science and Technology,
Hwarangno 14-gil 5, Seongbuk-gu,
Seoul 136-791, Republic of Korea
e-mail: swhong@kist.re.kr

K.-B. Lee
Department of Chemical and Biological Engineering,
Korea University,
Seoul 136-701, Republic of Korea

D.-J. Kim
Department of Earth and Environmental Sciences,
Korea University,
Seoul 136-701, Republic of Korea

1 Introduction

Phosphorus is an essential nutrient for the growth of organisms in ecosystems. It is the most important resource in many fields, such as the manufacture of fertilizers and detergents, and in pigment formulation. However, the increased discharge of nutrients, such as phosphate, into the water system contributes to eutrophication. The extensive uses of phosphate in various fields inevitably lead to huge amounts of phosphorus-containing water, and this has affected the water quality. Depletion of the oxygen level in a water body can be caused by eutrophication (Biswas et al. 2008) and gives rise to environmental degradation and has significant economic influences on drinking water supplies and fisheries (Rosenquist et al. 2010). For this reason, it has become necessary to evaluate the capacities of cost-effective techniques for the removal of phosphate.

Conventional methods for the removal of phosphate from water include chemical precipitation (Suzuki et al. 2007; Pastor et al. 2008), biological processes (Li et al. 2003; Oehmen et al. 2007), and adsorption processes (Pan et al. 2009; Park and Jung 2011). Activated sludge and biological nutrient removal, as biological treatments,

have been used for the removal of phosphate. However, these require strict controls, and it is difficult to obtain stable removal efficiency (Zhao and Sengupta 1998). Although chemical treatment has been widely used as an alternative to the biological method, this is expensive, with additional residual sludge treatment and disposal required. Conversely, adsorption techniques using appropriate adsorbents are promising, due to the production of less sludge, easy operation, and high efficiency (Cheng et al. 2009). Therefore, the removal of phosphate using various adsorbents, such as red mud (Lĭopez et al. 1998), alum sludge (Galarneau and Gehr 1997), apatite (Kandah 2004), and clinoptilolite (Tillman et al. 2005), has received increased attention.

One of the traditional applications of porous materials is for adsorption, including separation. Especially mesoporous materials, with high surface areas, large pore volumes, and a controlled pore size, can serve as a high performance support for adsorbents (Yang et al. 2007). The mesoporous structures of zirconium sulfate and titanium oxysulfate, synthesized using surfactants as a template, have shown high adsorption capacities for phosphate in aqueous solution under various pH conditions (Yeon et al. 2008; Choi et al. 2011). Although these mesoporous structures have high adsorption capacities for phosphate, the high cost of the base materials severely limits their application for commercial purposes.

The physical and chemical properties of silica-based mesoporous materials have recently been improved via surface modification using organic functional groups which has extended their applications (Sayari and Hamoudi 2001; Liu et al. 2009). These groups can be included via post-synthetic grafting or co-condensation during their syntheses (Hodgkins et al. 2005). Of these mesoporous materials, SBA-15 as base material has received attention for its highly ordered hexagonal structure, thermal stability, and dense walls compared with MCM-41 materials (Hoang et al. 2010).

In the present study, the application and characteristics of amino-functionalized SBA-15 synthesized through post-synthetic grafting and co-condensation methods, as well as pure SBA-15 for the removal of phosphate from sewage, were investigated and compared. The effects of contact time, phosphate concentration, and adsorbent dosage on the adsorption capacities of these modified and pure mesostructure adsorbents were examined to determine the equilibrium time and analyze the adsorption kinetics.

2 Materials and Methods

2.1 Chemicals

The mesoporous SBA-15 was synthesized using tetraethyl orthosilicate (TEOS, Aldrich, Korea) as the base silica source, with a tri-block poly(ethylene oxide)-poly (propylene oxide)-poly(ethylene oxide) ($EO_{20}PO_{70}EO_{20}$, P123, Aldrich, Korea) as the surfactant. Hydrochloric acid was obtained from Wako Pure Chemical Industries Ltd. 3-Aminopropyltrimethoxysilane was purchased from Sigma–Aldrich. Potassium phosphate, sodium hydroxide, potassium chloride, and ethanol were all from Sigma–Aldrich.

2.2 Pure SBA-15

Four grams of the amphiphilic tri-block copolymer, P123, was dispersed in 30 g of distilled water, stirred for 4 h, and 120 g of 2 M hydrochloric acid solution was then added, with the mixture then stirred for a further 2 h. TEOS was then added to the homogenous mixed solution, under stirring for 24 h at 40°C. The gel solution was transferred into a bottle and heated at 100°C for 24 h under static conditions. After the synthesis reaction, the solid was filtered, washed with distilled water, and dried in an air oven at 100°C for 5 h, followed by calcination at 540°C to remove the triblock copolymer (Zhao et al. 2000).

2.3 Preparation of Amino-Functionalized SBA-15 Using the Post-synthetic Grafting Method

Pure inorganic SBA-15 was synthesized via the method outlined in Section 2.2. One gram of dehydrated SBA-15 was stirred vigorously in 200 ml of 0.1 mol 3-aminopropyltriethoxysilane (APTES) for 24 h. The powder was collected by filtration, washed with distilled water, and dried at 60°C for 6 h. The obtained SBA-15, amino-functionalized with APTES via the post-synthetic grafting method, was designated as "post-synthetic grafting" (Zhao et al. 2011).

2.4 Preparation of Amino-Functionalized SBA-15 Using the Co-condensation Method

The synthesis of SBA-15, amino-functionalized with APTES through the co-condensation method, was

conducted as follows: Four grams of P123 and 8 g of potassium chloride were dissolved in 30 ml of distilled water and 120 ml of a 2-M hydrochloric acid solution at 40°C. Then, 8.5 g of TEOS was added, allowed to hydrolyze for 2 h, with 1.08 g of 3-aminopropyltrimethoxysilane then added. The 3-aminopropyltrimethoxysilane/TEOS molar ratio was 0.15. The mixed solution was stirred at room temperature for 20 h and then heated at 100°C for 24 h under static conditions. The white precipitate was filtered, washed with distilled water, followed by ethanol, and then dried under vacuum. To entirely remove the surfactant from the as-synthesized sample, 1 g of the ethanol-extracted material was stirred in 50 ml of aqueous 0.1 M hydrochloric acid for 1 h, filtered and dried, and

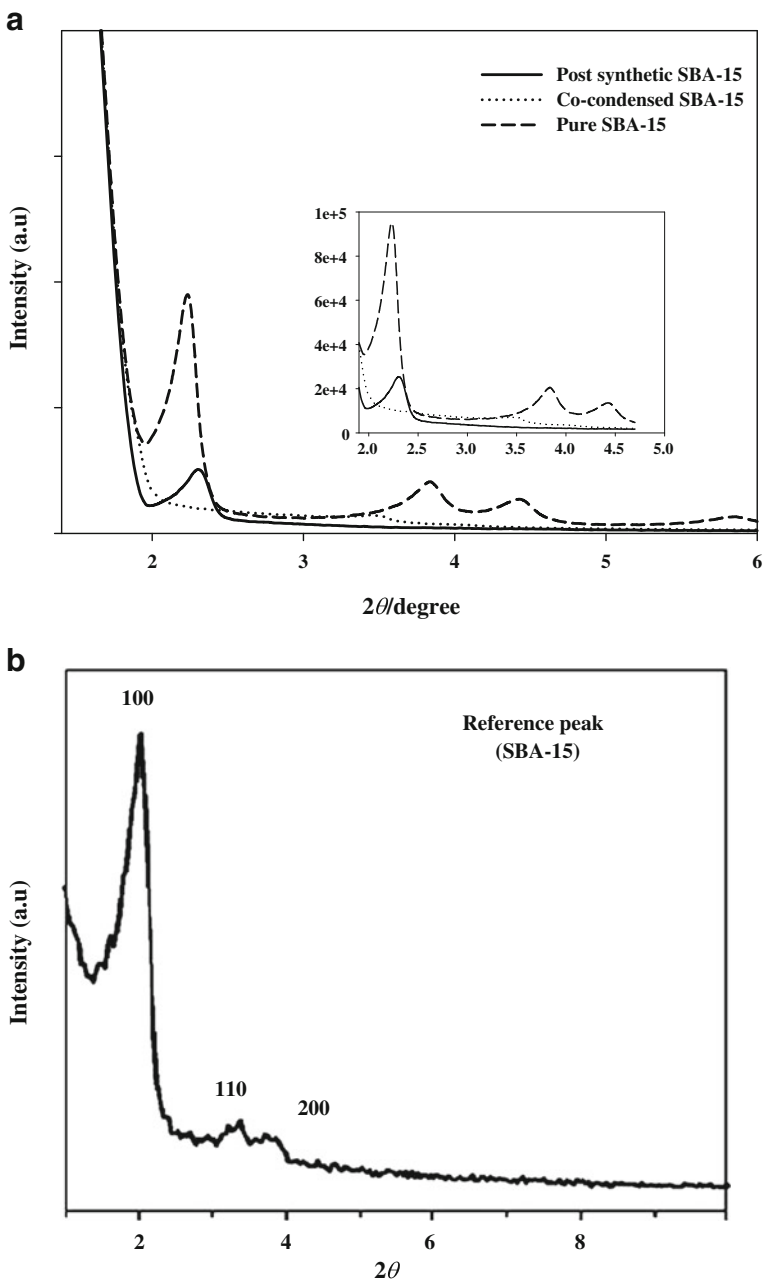

Fig. 1 X-ray diffraction patterns of **a** the post-synthetic grafting, co-condensed, and pure SBA-15 in this study and **b** pure SBA-15 in the reference

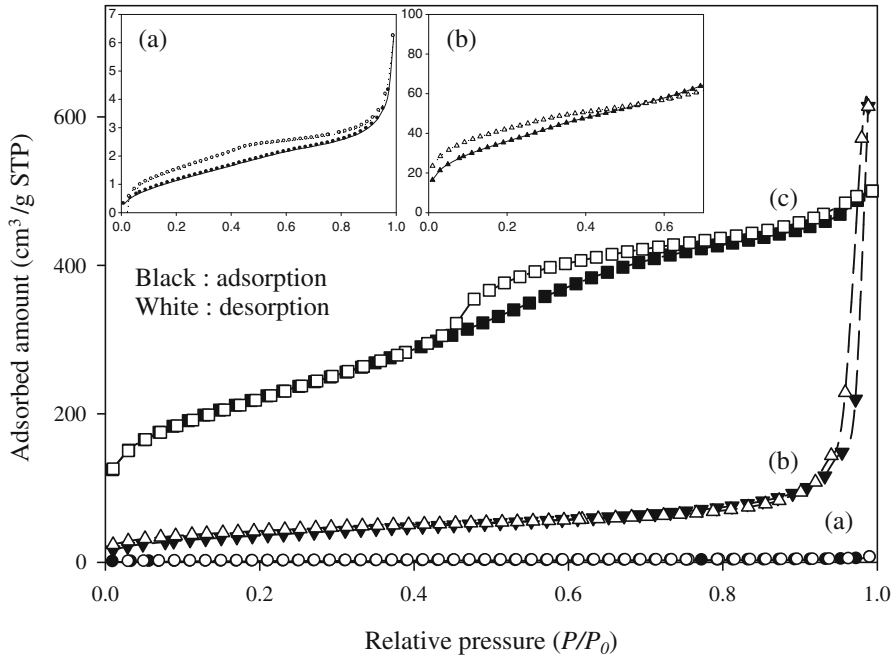

Fig. 2 Nitrogen adsorption/desorption isotherms for: **a** post-synthetic grafting, **b** co-condensed, and **c** pure SBA-15

then neutralized in 50 ml of 0.1 M sodium bicarbonate for 1 h. As the final step, the final solution was filtered and dried under vacuum at 100°C for 3 h. The obtained SBA-15, amino-functionalized through the co-condensation method, was designated as "co-condensation" (Da'na and Sayari 2011).

2.5 Experimental Process and Adsorption Model

2.5.1 Equilibrium Adsorption Test

The maximum adsorption capacities of the three mesostructures were estimated using adsorption isotherm tests. Fifty milliliters of phosphate solution, with initial concentrations of 5, 25, 50, 75, and 100 mg/l, was placed into 50-ml conical tubes containing 0.1 g of each of the adsorbents, i.e., post-synthetic grafting, co-condensation, and pure SBA-15. The phosphate solution was prepared by dissolving monopotassium phosphate (KH_2PO_4) in distilled water under pH 7.5. All samples were kept in an air-shaking incubator at 200 rpm, 20°C. After the reaction reached the equilibrium stage (1 h), the phosphate concentrations in the solutions were analyzed.

Table 1 Characterization data of the mesostructures

	S_{BET} (m^2/g)	V_P (cm^3/g)	$2R_P$[a] (nm)
Post-synthetic grafting SBA-15	211.4161	0.3728	2.7559
Co-condensation SBA-15	118.6919	0.0636	2.1439
SBA-15	789.8836	0.7736	3.9176

[a] BJH pore size analysis

2.5.2 Kinetic Adsorption Test

The three mesostructures, post-synthetic grafting, co-condensation, and pure SBA-15, were prepared for kinetic batch experiments. For each test tube, 50 mg of adsorbent was added to each 50-ml test tube, containing 50 mg/l of aqueous phosphate. The tubes were shaken in a shaking incubator at 200 rpm. Triplicate samples were routinely obtained from each tube using a microsyringe, at predetermined time intervals, and filtered through 0.45-μm membrane filters. The kinetic batch tests were continued for 60 min, after which the concentrations of aqueous phosphate showed no changes.

2.5.3 Modeling of Adsorption Isotherm

In order to quantify the adsorption capacities and time-dependent decreasing adsorption patterns of

the post-synthetic grafting, co-condensation, and pure SBA-15, equilibrium and kinetic adsorption models were used, following the Langmuir and Freundlich adsorption isotherm models (Eqs. 1 and 2) and three kinetic models (pseudo-first/second/third-order) (Eqs. 3, 4, 5, 6, and 7) (Peleka and Deliyanni 2009), as follows:

$$S = \frac{\alpha\beta C}{1 + \alpha C} \tag{1}$$

$$q = KC^{1/n} \tag{2}$$

where S and C are the adsorbed and residual aqueous concentrations, and α and β, the constants related with the binding energy (l/mg) and the maximum adsorption capacity (milligrams per kilogram), respectively. q is the amount adsorbed at equilibrium (milligrams per gram).

$$\log(q_e - q_t) = \log(q_e) - \frac{k_1}{2.303} t \tag{3}$$

where k_1 is the rate constant of pseudo-first-order adsorption (1/min), q_e the amount of phosphate sorbed at equilibrium (milligrams per gram), and q_t the amount of phosphate sorbed at time t (milligrams per gram).

$$\frac{dq_t}{dt} = k_2(q_e - q_t)^2 \tag{4}$$

where k_2 is the second-order reaction constant, q_e the amount of phosphate sorbed at equilibrium (milligrams per gram), and q_t the amount of phosphate sorbed at time t (milligrams per gram). When Eq. 3 is integrated, the following equation is obtained:

$$\frac{1}{q_e - q_t} = k_2 t + C_2 \tag{5}$$

In Eq. 4, C_2 is the integration constant, and with an algorithmic arrangement, the following expression is developed (Peleka and Deliyanni 2009):

$$\frac{t}{q_t} = \frac{1}{k_2 q_e^2} + \frac{t}{q_e} \tag{6}$$

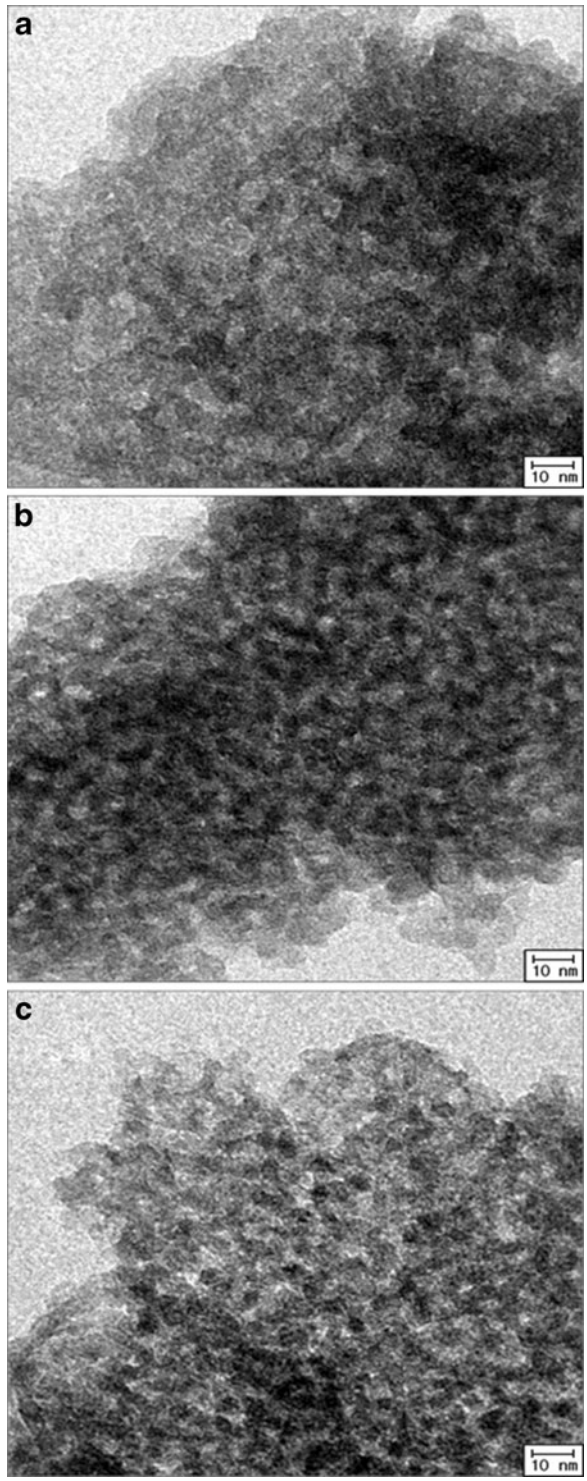

Fig. 3 Transmission microscope images of: **a** post-synthetic grafting, **b** co-condensed, and **c** pure SBA-15

Considering one adsorbate was sorbed onto three surface sites of the examined materials, the sorption rate equation would be as shown below:

$$q_t = q_0 - (q_0 - q_e)[1 - \frac{1}{(1 + 2k_3 t)^{\frac{1}{2}}}] \quad (7)$$

where k_3 is the third-order reaction constant (1/min).

2.6 Analytical Methods

2.6.1 Characterization of Mesostructures

The surface areas of the mesostructured adsorbents were calculated using the Brunauer–Emmet–Teller (BET) equation, with the pore size distribution calculated using the Barrett–Joyner–Halenda (BJH) method, employing the desorption branch of the isotherm. Powder X-ray diffraction (XRD) patterns of the adsorbents were obtained within the range 1.0° to 90.0°, in steps of 0.02° (D-MAX 2500, Rigaku, Japan). Transmission electron microscope (TEM) images were obtained using TEM equipment (JEM-2200FS, JEOL, Japan). Fourier transform infrared spectroscopy (FT-IR) spectra were run using a Mattson Infinity Gold FT-IR spectrometer, with a frequency resolution of 4.0 cm^{-1}.

2.6.2 Phosphate Measurement

The phosphate concentration was analyzed by ion chromatography (ICS-1000, DIONEX, USA). The phosphate solution was separated from the solids using 0.45-μm membrane filters, and then the residual phosphorus concentrations were analyzed.

3 Results and Discussion

3.1 Characterization of the Adsorbents

The small-angle X-ray diffraction patterns of the post-synthetic grafting, co-condensation, and pure SBA-15 are shown in Fig. 1. For the case of pure SBA-15, three resolved diffraction peaks, with 2θ at 0.90, 1.54, and 1.74°, were observed, corresponding to the (100), (110), and (200) planes (Jiang et al. 2007). These indicated the presence of a typical hexagonal mesostructure (Esparza et al. 2004). In comparison with pure SBA-15, the post-synthetic grafting and co-condensation methods caused decreased peak intensities due to the partial loss of the space correlation of the pores which has been observed in many investigations (Yoshitake et al. 2002; Kao et al. 2008; Hu et al. 2009). In addition, the positions of the peaks were shifted to slightly higher angles by silylation (Yokoi et al. 2004). However, the ordered structures of meso-materials were observed to be well maintained after the functionalization.

The nitrogen adsorption–desorption isotherms of the (a) post-synthetic grafting, (b) co-condensation, and (c) pure SBA-15 are presented in Fig. 2. In all cases, the nitrogen adsorption/desorption isotherms

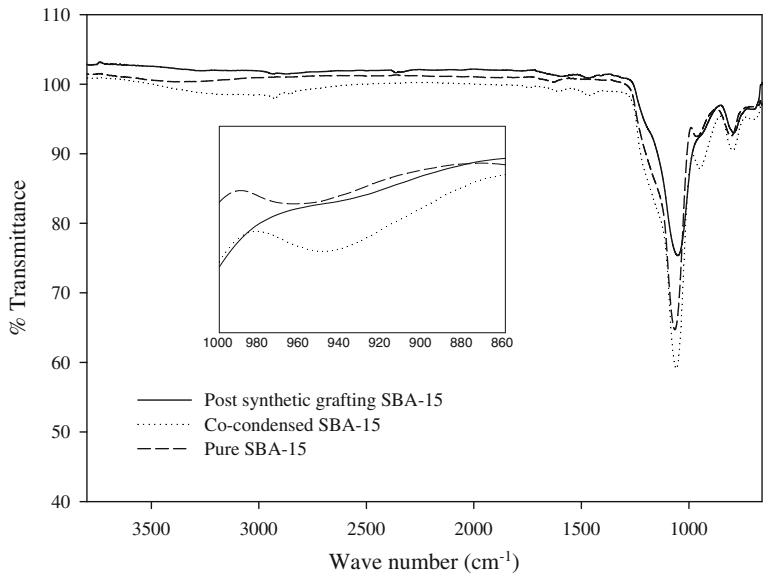

Fig. 4 FT-IR spectra of: **a** post-synthetic grafting, **b** co-condensed, and **c** pure SBA-15

exhibited type IV, implying that the mesostructure was highly stable under various pH conditions, especially that of pure SBA-15. A portion of the adsorption occurred between $0.1<P/P_0<0.9$ in the isotherms for (a) post-synthetic grafting and between $0.0<P/P_0<0.4$ for (b) co-condensation SBA-15. A significant hysteresis appears slightly in the adsorption/desorption isotherms for these catalysts. However, a marked step appeared between $0.5<P/P_0<0.7$ for pure SBA-15, with typical hysteresis. This feature is indicative of the specific presence of a mesoporous structure. Upon grafting and co-condensation to the framework walls, significant decreases in the surface areas, pore volumes, and pore sizes were observed due to the bidentate diamino group ligand on the framework channels. This type of pattern has been observed in MCM-41 and SBA-1, where the pore size distributions at the boundary were found to be within the meso-range (Sayari and Hamoudi 2001; Yoshitake et al. 2002). The BET surface area, pore volume, and pore size in the BJH distributions are listed in Table 1. The surface areas of the post-synthetic grafting, co-condensation, and pure SBA-15 were calculated

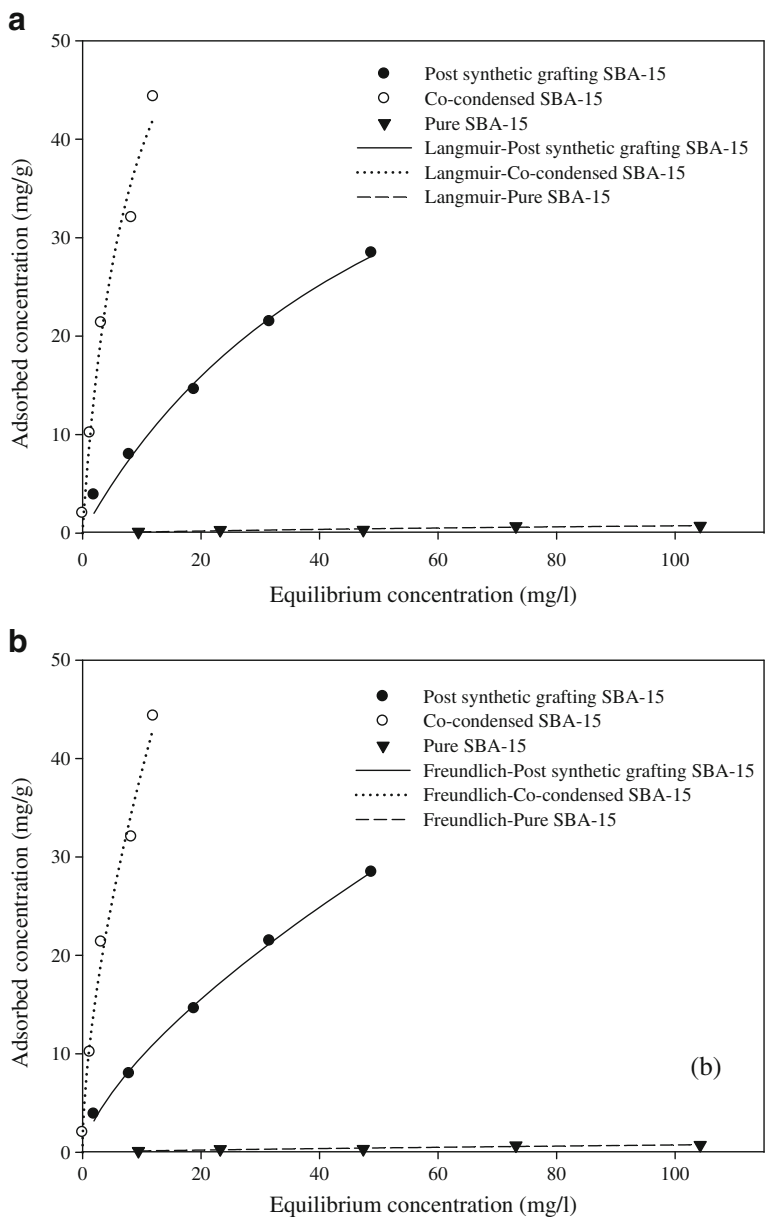

Fig. 5 The adsorption of phosphate onto the mesostructures fitted with the **a** Langmuir and **b** Freundlich isotherms

Table 2 Estimated isotherm parameters for the adsorption of phosphate onto the three mesostructures

Langmuir equation ($S=\alpha\beta C/(1+\alpha C)$)				
	β (mg P/g)	α (l/mg)	R^2	SE
Post-synthetic grafting SBA-15	59.890	0.0181	0.9890	1.2032
Co-condensation SBA-15	69.970	0.0530	0.9782	2.8799
SBA-15	2.018	0.0057	0.9106	0.0922
Freundlich equation ($q=KC^{1/n}$)				
	K	$1/n$	R^2	SE
Post-synthetic grafting SBA-15	2.0423	0.6778	0.9980	0.5094
Co-condensation SBA-15	9.6564	0.6030	0.9857	2.3311
SBA-15	0.0231	0.7523	0.9123	0.0913

211.4161, 118.6919, and 789.8836 m^2/g, respectively. Decreases in the mesoporous diameters and pore volumes were also observed. These results indicated that the modification to the SBA-15 had been successful.

The transmission electron microscope images for the three samples exhibited hexagonal arrangements, as shown in Fig. 3. Figure 3a, b, and c represent the post-synthetic grafting, co-condensation, and pure SBA-15. The TEM images showed that the mesoporous diameters of post-synthetic grafting and co-condensation were slightly narrower than that before modification. However, the pore sizes of the grafting and co-condensation SBA-15 were about 0.70 and 0.55 times smaller, respectively, than that of pure SBA-15. These observations were in good agreement with the results obtained from the XRD analysis.

The FT-IR spectra of the post-synthetic grafting, co-condensation, and pure SBA-15 are shown in Fig. 4. In the case of pure SBA-15, the broad band at 3,200–3,500 cm^{-1} was associated with the surface hydroxyl groups (O–H). However, instead of a hydroxyl group peak, the characteristic peak of aminosilane, such as C–H asymmetric stretching, was shown at around 2,800–3,000 cm^{-1} in the co-condensation SBA-15 (Bae et al. 2009). The small intensities of the peaks at 1,350–1,500 cm^{-1}, due to the P123 surfactant residues, were weak (Hu et al. 2009). Bands were observed at 1055, 790, and 695 cm^{-1} in the spectrum after grafting, which were attributed to C–N, N–H wagging, and amine function (N–H), respectively. These results imply the amine functional group had been attached well to the surface of the SBA-15 by the grafting method, as well as being chemically incorporated into the frameworks of the ordered mesoporous material via the co-condensation (Hu et al. 2009).

3.2 Equilibrium Adsorption

In order to compare the phosphorus removal efficiencies, fitting of the experimental data was performed. Figure 5a and b shows the Langmuir and Freundlich adsorption isotherms of phosphate onto the three mesostructures, i.e., post-synthetic grafting, co-condensation, and pure SBA-15. In the study of the sorption of phosphate onto adsorbents, it has been found that a plot of the adsorption concentration (C^*) versus equilibrium (C_{eq}) will yield a curve with a modified hyperbola and power type. Both of the adsorption isotherms resulted in

Table 3 Adsorption constants of the Langmuir isotherm for phosphate

Langmuir equation	Post-synthetic grafting SBA-15[a]	Co-condensation SBA-15[a]	SBA-15[a]	Coal ash (Yan et al. 2007)	Clay soil (Hamdi and Srasra 2008)	Aluminum oxide (Zhang et al. 2010)
α (l/mg)	0.02	0.05	0.01	0.01	6.18×10^{-4}	0.61
β (mg/g)	59.89	69.97	2.02	28.60	31.84	14.80
Freundlich equation						
K	2.04	9.66	0.02	6.80	0.03	6.90
$1/n$	0.68	0.60	0.75	0.74	0.88	0.21

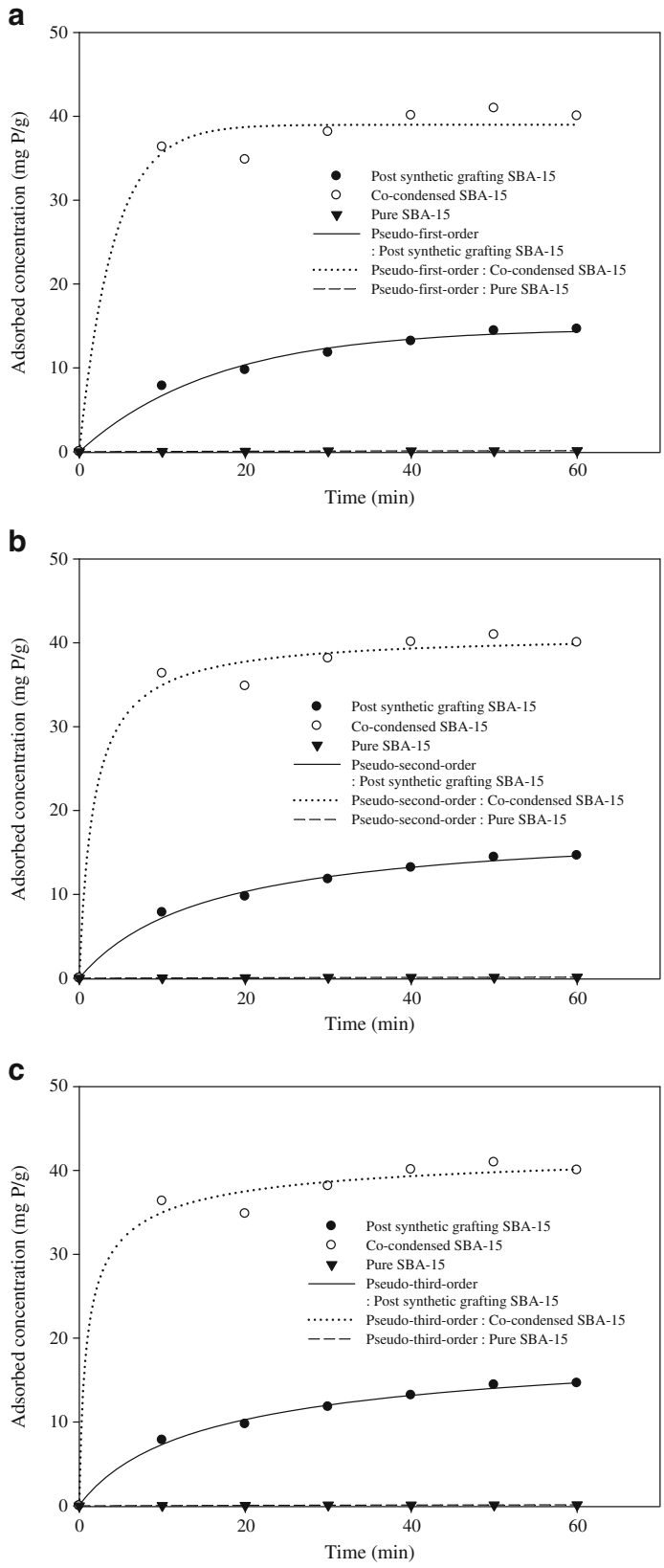

Fig. 6 The adsorption of phosphate onto the meso-structures fitted with the pseudo- **a** first, **b** second, and **c** third-order kinetic adsorption model

nonlinear curves, with an asymptotic increase. The R^2 values found for the Freundlich isotherm were found to be slightly higher than those for the Langmuir isotherm, but both models gave high R^2 values, ranging from 0.978 to 0.998, with the exception of pure SBA-15, which gave an R^2 value of 0.910 (Table 2). The slopes of the curves for co-condensed SBA-15 were the steepest for phosphate until saturation, while aqueous phosphate was barely removed by pure SBA-15 (Fig. 5a). The slope was found to be significantly dependent on the type of mesostructure. In the case of the maximum adsorption capacities, post-synthetic SBA-15 also had the highest value (Table 2). The maximum adsorption is proportional to binding energy (α) and slope of the curve, but not the surface area (S_{BET}). For the Langmuir equation, the maximum adsorption capacity (β) of co-condensed SBA-15 was found to be 69.970 mg/g, which was higher than those of post-synthetic grafting and pure MCM-41. This value was also higher than the 28.60 (Yan et al. 2007), 31.84 (Hamdi and Srasra 2008), and 14.80 mg/g (Zhang et al. 2010) for the adsorption capacities of coal ash, various clay soils, and aluminum oxide, respectively, reported in the literature (Table 3). Conversely, for the Freundlich equation, the data showed that the K constant remained higher for the co-condensed SBA-15 than for the two other mesostructures used in this study, as well as for other adsorbents reported in the literature (Table 3). The values of $1/n$ were within the range 0.1 and 1.0. This means that suitable adsorption of phosphate would be achieved by all adsorbents (Boujelben et al. 2008).

The results of the equilibrium adsorption test showed that the Freundlich equation gave slightly better fits than the Langmuir equation for the adsorption equilibrium data over the concentration range used in this study. This fact may indicate that the adsorbents used in this study underwent a multilayer for the adsorption process (Akar et al. 2009).

3.3 Adsorption Kinetics

In order to elucidate the mechanism of phosphate adsorption, various kinetic models, the nonlinear form of the pseudo-first/second/third-order kinetics models, were applied to the obtained results (Fig. 6a–c). The data showed that the adsorptions of phosphate onto the post-synthetic grafting and co-condensation SBA-15 were very fast, with equilibria attained after 30 and 15 min, respectively. In the case of pure SBA-15, very little phosphate had been removed from solution after the reaction. The differences in the adsorption capacities of each adsorbent can be related to the differences in their methods of synthesis. The kinetic parameters, such as the adsorption constants, correlation coefficients, and predicted and experimental q_e values for the pseudo-first/second/third-order model, are summarized in Table 4. Also, to distinguish which of these three kinetic models was the most appropriate, a comparison between the theoretical and experimental adsorption capacities from the kinetic adsorption test was conducted. Although high correlation coefficients were obtained for each model, the adsorptions of phosphate onto the post-synthetic grafting, co-condensation, and pure SBA-15 closely matched the predicted q_e of pseudo-first-order kinetics (Azizian 2004). As a result, the process appeared to follow pseudo-first-order kinetics, with the use of this model appearing to be a dependable method for predicting the absorption of phosphate according to the reaction time.

3.4 Phosphate Removal Efficiency by the Post-synthetic Grafting, Co-condensation, and Pure SBA-15

The maximum adsorption capacity of phosphate by co-condensed SBA-15 was higher than those for the post-synthetic grafting and pure material. The removal efficiency of phosphate in this study was affected by

Table 4 Kinetic parameters for the mesostructures synthesized using different methods

Material	$q_{e\ exp}$ (mg/g)	Pseudo-first-order model			Pseudo-second-order model			Pseudo-third-order model		
		k_1	$q_{e\ mod}$	R^2	k_2	$q_{e\ mod}$	R^2	k_3	$q_{e\ mod}$	R^2
Post-synthetic grafting SBA-15	14.62	0.0610	14.72	0.9982	0.0035	18.37	0.9935	0.0586	22.64	0.9950
Co-condensation SBA-15	40.03	0.2456	38.99	0.9827	0.0141	41.02	0.9898	1.1899	43.78	0.9913
SBA-15	0.12	0.0187	0.18	0.9750	0.0414	0.29	0.9746	0.0086	0.40	0.9745

the following factors. Co-condensation (one-pot synthesis) is an alternative method for the synthesis of functionalized mesoporous silica phases. Because the organic functionalities are direct components of the silica matrix, pore blocking does not pose a problem with the co-condensation method. In addition, the organic functional compounds were more homogeneously distributed than those via the post-synthetic grafting process (Kao et al. 2008). On the contrary, the post-synthetic grafting method refers to the subsequent modification of the inner surfaces of mesoporous silica phases with organic compounds. This method has the advantage that the mesostructure of the base material, such as SBA-15 or MCM-41, is retained, whereas, the lining of the walls causes a reduction in the porosity (Hoffmann et al. 2006). Although the porosity was decreased and the adsorption capacity of pure SBA-15 was only slight, the chemical affinity of the amine adhered as a functional group onto the inner pore surface was responsible for the higher removal efficiency. Consequently, these characteristics, formed by the synthesis methods, lead to the above-mentioned results.

4 Conclusions

In this study, experiments were conducted to investigate the applicability of three mesostructures, i.e., post-synthetic grafting, co-condensation, and pure SBA-15, as adsorbents for the removal of phosphate from sewage. The co-condensed SBA-15 was found to be more efficient for the adsorption of phosphate compared to the other two adsorbents. The equilibrium adsorption isotherms were well fitted not only to the Langmuir model, but also to the Freundlich model; however, there were slight differences. The maximum adsorption capacity was found to be 69.970 mg/g when using co-condensation material, but 59.890 mg/g for the post-synthetic and 2.018 mg/g for pure SBA-15. The adsorption capacity of SBA-15 and the chemical affinity for the adhered amine, as a functional group, onto the inner pore surfaces were the cause of the higher removal efficiency compared with pure SBA-15. The kinetic data were analyzed using pseudo-first/second/third models, which showed the adsorptions of phosphate onto the three different mesostructures followed the pseudo-first-order kinetic model. The results obtained from the kinetic studies indicated that the reaction time was appropriate for the technological application of these materials. This study gave promising results for the application of the amino-functionalized mesostructure as an adsorbent for the adsorption of phosphate from aqueous solution. Further experiments should involve the regeneration of the amine functionalized SBA-15 for reuse and to achieve more cost-effective phosphate removal.

Acknowledgments The subject is supported by the Korea Ministry of Environment as “Global Top Project” (project no.: GT-11-B-01-011-1).

References

Akar, S. T., Özcan, A. S., Akar, T., Özcan, A., & Kaynak, Z. (2009). Biosorption of a reactive textile dye from aqueous solutions utilizing an agro-waste. *Desalination, 249*, 757–761.

Azizian, S. (2004). Kinetic models of sorption. A theoretical analysis. *Journal of Colloid and Interface Science, 276*, 47–52.

Bae, J. A., Song, K. C., Jeon, J. K., Ko, Y. S., Park, Y. K., & Yim, J. H. (2009). Effect of pore structure of amine-functionalized mesoporous silica-supported rhodium catalysts on 1-octene hydroformylation. *Microporous and Mesoporous Materials, 123*, 289–297.

Biswas, B. K., Inoue, K., Ghimire, K. N., & Harada, H. (2008). Removal and recovery of phosphorus from water by means of adsorption onto orange waste gel loaded with zirconium. *Bioresource Technology, 99*, 8685–8690.

Boujelben, N., Bouzid, J., Elouear, Z., Feki, M., Jamoussi, F., & Montiel, A. (2008). Phosphorus removal from aqueous solution using iron coated natural and engineered sorbents. *Journal of Hazardous Materials, 151*, 103–110.

Cheng, X., Huang, X., Wang, X., Zhao, B., Chen, A., & Sun, D. (2009). Phosphate adsorption from sewage sludge filtrate using zinc-aluminum layered double hydroxides. *Journal of Hazardous Materials, 169*, 958–964.

Choi, J. W., Lee, S. Y., Park, K. Y., Lee, K. B., Kim, D. J., & Lee, S. H. (2011). Investigation of phosphate removal from wastewater through ion exchange of mesostructure based on inorganic material. *Desalination, 266*, 281–285.

Da'na, E., & Sayari, A. (2011). Adsorption of copper on amine-functionalized SBA-15 prepared by co-condensation: Equilibrium properties. *Chemical Engineering Journal, 166*(1), 445–453.

Esparza, J. M., Ojeda, M. L., Campero, A., Dominguez, A., Kornhauser, I., Rojas, F., Vidales, A. M., Lopez, R. H., & Zgrablich, G. (2004). N_2 sorption scanning behavior of SBA-15 porous substrates. *Colloids and Surfaces A: Physicochem. Eng. Aspects, 241*, 35–45.

Galarneau, E., & Gehr, R. (1997). Phosphorus removal from wastewaters: Experimental and theoretical support for alternative mechanisms. *Water Research, 31*(2), 328–338.

Hamdi, N., & Srasra, E. (2008). Sorption of phosphate from acidic wastewater into three Tunisian type clay soils. *Journal of Water Chemistry and Technology, 30*(4), 208–214.

Hoang, V. D., Dang, T. P., Dinh, Q. K., Nguyen, H. P., & Vu, A. T. (2010). The synthesis of novel hybrid thiol-functionalized nano-structured SBA-15. *Advances in Natural Sciences: Nanoscience and Nanotechnology, 1*, 1–6.

Hodgkins, R. P., Garcia-Bennett, A. E., & Wright, P. A. (2005). Structure and morphology of propylthiol-functionalised mesoporous silica templates by non-ionic triblock copolymers. *Microporous and Mesoporous Materials, 79*, 241–252.

Hoffmann, F., Cornelius, M., Morell, J., & Fröba, M. (2006). Silica-based mesoporous organic-inorganic hybrid materials. *Angewandte Chemie International Edition, 45*, 3216–3251.

Hu, Q., Li, J. J., Hao, Z. P., Li, L. D., & Qiao, S. Z. (2009). Dynamic adsorption of volatile organic compounds on organofunctionalized SBA-15 materials. *Chemical Engineering Journal, 149*, 281–288.

Jiang, Y., Gao, Q., Yu, H., Chen, Y., & Deng, F. (2007). Intensively competitive adsorption for heavy metal ions by PAMAM-SBA-15 and EDTA-PAMAM-SBA-15. *Microporous and Mesoporous Materials, 103*, 316–324.

Kandah, M. L. (2004). Zinc and cadmium adsorption on low-grade phosphate. *Separation and Purification Technology, 35*, 61–70.

Kao, H. M., Liao, C. H., Palani, A., & Liao, Y. C. (2008). One-pot synthesis of ordered and stable cubic mesoporous silica SBA-1 functionalized with amino functional groups. *Microporous and Mesoporous Materials, 113*, 212–223.

Li, J., Xing, X. H., & Wang, B. Z. (2003). Characteristics of phosphorous removal from wastewater by biofilm sequencing batch reactor (SBR). *Biochemical Engineering Journal, 16*, 279–285.

Lĭopez, E., Soto, B., Arias, M., Nĭŭnez, A., Rubinos, D., & Barral, T. (1998). Adsorbent properties of red mud and its use for wastewater treatment. *Water Research, 32*(4), 1314–1322.

Liu, D., Lei, J. H., Guo, L. P., Du, X. D., & Zeng, K. (2009). Ordered thiol-functionalized mesoporous silica with macrostructure by true liquid crystal templating route. *Microporous and Mesoporous Materials, 117*, 67–74.

Oehmen, A., Lemos, P. C., Carvalho, G., Yuan, Z. G., Keller, J., Blackall, L. L., & Reis, M. A. M. (2007). Advances in enhanced biological phosphorus removal: From micro to macro scale. *Water Research, 41*, 2271–2300.

Pan, B., Wu, J., Pan, B., Lv, L., Zhang, W., Xiao, L., Wang, X., Tao, X., & Zheng, S. (2009). Development of polymer-based anaosized hydrated ferric oxides (HFOs) for enhanced phosphate removal from waste effluents. *Water Research, 43*, 4421–4429.

Park, J. H., & Jung, D. I. (2011). Removal of total phosphorus (TP) from municipal wastewater using loess. *Desalination, 269*, 104–110.

Pastor, L., Mangin, D., Barat, R., & Seco, A. (2008). A pilot-scale study of struvite precipitation in a stirred tank reactor: Conditions influencing the process. *Bioresource Technology, 99*, 6285–6291.

Peleka, E. N., & Deliyanni, E. A. (2009). Adsorptive removal of phosphates from aqueous solutions. *Desalination, 245*, 357–371.

Rosenquist, S. E., Hession, W. C., Eick, M. J., & Vaughan, D. H. (2010). Variability in adsorptive phosphorus removal by structural stormwater best management practices. *Ecological Engineering, 36*, 664–671.

Sayari, A., & Hamoudi, S. (2001). Periodic mesoporous silica-based organic-inorganic nanocomposite materials. *Chemisty of Materials, 13*, 3151–3168.

Suzuki, K., Tanaka, Y., Kuroda, K., Hanajima, D., Fukumoto, Y., Yasuda, T., & Waki, M. (2007). Removal and recovery of phosphorous from swine wastewater by demonstration crystallization reactor and struvite accumulation device. *Bioresource Technology, 98*, 1573–1578.

Tillman, F. D., Bartelt-Hunt, S. L., Craver, V. A., Smith, J. A., & Alther, G. R. (2005). Relative metal ion sorption on natural and engineered sorbents: Batch and column studies. *Environmental Engineering Science, 22*, 400–409.

Yan, J. Y., Kirk, D., Jia, C. Q., & Liu, X. (2007). Sorption of aqueous phosphorus onto bituminous and lignitous coal ashes. *Journal of Hazardous Materials, 148*, 395–401.

Yang, L., Wang, Y., Huang, D., Luo, G., & Dai, Y. (2007). Preparation of high performance adsorbents by functionalizing mseostructured silica spheres for selective adsorption of organosulfur compounds. *Industrial and Engineering Chemistry Research, 46*, 579–583.

Yeon, K. H., Park, H. S., Lee, S. H., Park, Y. M., Lee, S. H., & Iwamoto, M. (2008). Zirconium mesostructures immobilized in calcium alginate for phosphate removal. *Korean Journal of Chemical Engineering, 25*(5), 1040–1046.

Yokoi, T., Tatsumi, T., & Yoshitake, H. (2004). Fe^{3+} coordinated to amino-functionalized MCM-41: An adsorbent for the toxic oxyanions with high capacity, resistibility to inhibiting anions, and reusability after a simple treatment. *Journal of Colloid and Interface Science, 274*, 451–457.

Yoshitake, H., Yokoi, T., & Tatsumi, T. (2002). Adsorption of chromate and arsenate by amino-functionalized MCM-41 and SBA-1. *Chemistry of Materials, 14*, 4603–4610.

Zhang, L., Hong, S., He, J., Gan, F., & Ho, Y. S. (2010). Isotherm study of phosphorus uptake from aqueous solution using aluminum oxide. *Clean-Soil Air Water, 38*, 831–836.

Zhao, D., & Sengupta, A. K. (1998). Ultimate removal of phosphate from wastewater using a new class of polymeric ion exchangers. *Water Research, 32*, 1613–1625.

Zhao, D., Sun, J., Li, Q., & Stucky, G. D. (2000). Morphological control of highly ordered mesoporous silica SBA-15. *Chemistry of Materials, 12*, 275–279.

Zhao, Y., Gao, Q., Tang, T., Xu, Y., & Wu, D. (2011). Effective NH_2-grafting on mesoporous SBA-15 surface for adsorption of heavy metal ions. *Materials Letters, 65*(6), 1045–1047.